

RESEARCH REPORT

WILEY

Paclitaxel alters the microvascular network in the central and peripheral nervous system of rats with chemotherapy-induced painful peripheral neuropathy

Antonio Giuliano Zippo¹ | Virginia Rodriguez-Menendez^{2,3} | Eleonora Pozzi^{2,3} | Annalisa Canta^{2,3} | Alessia Chiorazzi^{2,3} | Elisa Ballarini^{2,3} | Laura Monza^{2,3} | Paola Alberti^{2,3,4}  | Cristina Meregalli^{2,3}  | Alberto Bravin⁵ | Paola Coan⁶ | Elena Longo⁷ | Giulia Saccomano^{7,8} | Katrine Paiva⁹ | Giuliana Tromba⁷ | Guido Cavaletti^{2,3,4}  | Valentina Alda Carozzi^{2,3} 

¹Institute of Neuroscience, Consiglio Nazionale delle Ricerche, Monza, Italy

²Experimental Neurology Unit, School of Medicine and Surgery, University of Milano-Bicocca, Milan, Italy

³NeuroMI (Milan Center for Neuroscience), Milan, Italy

⁴Fondazione IRCCS San Gerardo dei Tintori, Monza, Italy

⁵Physics Department, University of Milano-Bicocca, Milan, Italy

⁶Faculty of Physics, Ludwig-Maximilian University, Munich, Germany

⁷Elettra-Sincrotrone Trieste S.C.p.A, Trieste, Italy

⁸Department of Architecture and Engineering, University of Trieste, Trieste, Italy

⁹Laboratory of Applied Physics to Biomedical Science, Physics Institute, Rio de Janeiro State University, Rio de Janeiro, Brazil

Correspondence

Valentina Alda Carozzi, Experimental Neurology Unit, School of Medicine and Surgery, University of Milano-Bicocca, Via Cadore 48, 20900 Monza, Italy.
Email: valentina.carozzi1@unimib.it

Funding information

Università degli Studi di Milano-Bicocca; Italian Government (Piano Complementare al Piano Nazionale di Ripresa e Resilienza); Associazione Italiana per la Ricerca sul Cancro; Italian Ministry of University and Research, Grant/Award Number: 2022NBS28K; FAR 2022–2021 University Grants, Grant/Award Number: IG2021; NRRP Complementary Investments, Grant/Award Number: PNC0000003

Abstract

Background and Aims: Chemotherapy-induced peripheral neurotoxicity (CIPN), with paraesthesia, numbness, dysesthesia and neuropathic pain ranks among the most common dose-limiting toxicity of several widely used anticancer drugs. Recent studies revealed the microvascular angiogenesis as a new important actor, beside peripheral neurons, in the neurotoxicity and neuropathic pain development and chronicisation. The aim of this work is to elucidate the role of vascular alterations in CIPN.

Methods: We evaluated the severity of CIPN with neurophysiological, behavioural and neuropathological analysis together with the microvascular network in central and peripheral nervous systems of rats in order to correlate the features of the CIPN and the vascular abnormalities. The vascular network was quantitatively evaluated through synchrotron radiation-based X-ray phase-contrast micro-tomography

Abbreviations: CDDP, cis-diamine-dichloroplatin; CIPN, chemotherapy-induced peripheral neurotoxicity; CNS, central nervous system; IENF, intra-epidermal nerve fibres; L4-L6 DRG, lumbar dorsal root ganglia; PNS, peripheral nervous system; PTX, paclitaxel; S1, S1 somatosensory cortex; SNAP, sensory nerve amplitude of the action potential; SNCV, sensory nerve conduction velocity; XPCT, X-ray phase-contrast micro-tomography.

This is an open access article under the terms of the [Creative Commons Attribution-NonCommercial-NoDerivs](https://creativecommons.org/licenses/by-nc-nd/4.0/) License, which permits use and distribution in any medium, provided the original work is properly cited, the use is non-commercial and no modifications or adaptations are made.

© 2024 The Author(s). *Journal of the Peripheral Nervous System* published by Wiley Periodicals LLC on behalf of Peripheral Nerve Society.

imaging, measuring four specific parameters: vascular density, vessel diameter, vessel tortuosity and branching.

Results: Rats exposed to paclitaxel and affected by a severe painful sensory axonopathy showed an increased vascular density (putative sprouting angiogenesis) in the crucial districts of the central (somatosensory cortex and lumbar spinal cord) and peripheral nervous system (lumbar dorsal root ganglia). In addition, the complexity of the vascular network and the size of neo-formed vessels were significantly decreased in specific regions. On the other hand, less significant changes were observed in rats exposed to cisplatin, affected by a painless peripheral neuropathy, suggesting a specific involvement of neo-angiogenesis in the development of severe neurotoxicity and neuropathic pain.

Interpretations: These new ground-breaking results can shed light on new pathogenetic mechanisms and potential novel therapeutic approaches for painful-CIPN.

KEYWORDS

angiogenesis, central nervous system, chemotherapy, microvessels, neurotoxicity, peripheral nervous system, X-ray microtomography

1 | INTRODUCTION

According to the data provided by the World Health Organization International Agency for Research on Cancer (<http://gco.iarc.fr>), more than 19 million people worldwide received a diagnosis of cancer in 2020. While in the last decades, cancer patients' life expectancy has substantially increased, chemotherapy still causes long-term, severe side effects that hit hundreds of thousands of people. The most urgent unmet needs for cure are toxicities involving peripheral (PNS) and central (CNS) nervous systems that have severe and often long-term debilitating consequences affecting 70% of those patients receiving neurotoxic chemotherapy.^{1,2} Chemotherapy-induced peripheral neurotoxicity (CIPN), with paraesthesia, numbness, dysesthesia and sensory ataxia ranks among the most common dose-limiting toxicity of several widely used anticancer drugs such as platinum and taxanes. Notably, neuropathic pain requiring medical treatment is reported by patients even years after therapy cessation³⁻⁵ and it is, only at least, tentatively treated according to international guidelines (for details, see the studies by Attal et al.,⁶ Bates et al.⁷ and Dworkin et al.⁸). It should be noted that among all drugs available for neuropathic pain treatment, only duloxetine showed moderate efficacy against neuropathic pain related to CIPN, and specifically paclitaxel-related CIPN.⁴ Taken together, these facts highlight the need for a better understanding and treatment of neurotoxicity and neuropathic pain due to CIPN. At the moment, effective neuroprotective strategies are not available so far and the only option to prevent severe and permanent neurological deficits is to reduce or withdraw the anticancer treatment, thus affecting the oncological patients' outcome.

The painful peripheral neuropathy is the result of peripheral nerve damage, which modifies the pain-processing neural circuits and involves neurons that become hypersensitized, a condition that

triggers long-term changes in many spinal, cortical and subcortical regions.⁹ Painful chemotherapy-induced peripheral neuropathy (painful-CIPN) can be considered a CIPN exacerbated by neuropathic pain measured as an altered response to mechanical and thermal stimuli. It is to note that not all neurotoxic chemotherapies that induce a peripheral neuropathy also produce painful conditions. For example, the principal symptoms of CIPN induced by cisplatin are paraesthesia, progressing to proprioceptive loss, areflexia and sensory ataxia, in high rates of patients receiving cumulative doses of cis-diamine-dichloroplatin (CDDP),¹⁰ other than neuropathic pain. Paclitaxel (PTX), on the other hand, induces numbness, tingling and neuropathic pain as allodynia (increased responsiveness to mild mechanical and thermal stimuli) in the patient's fingers, toes, lower leg, and wrist with a "glove and stocking" distribution (Klein and Lehmann, 2021).¹¹

Even if the huge number of studies performed so far (for comprehensive recent reviews see the studies by Alberti et al.,³ Bae et al.¹² and Zajaczkowska et al.¹³), CIPN pathogenesis remains elusive. Peripheral neurons (devoid of blood-brain barrier) have, for a long time, been considered the only reasonable target of investigations that led to the discovery of several pathogenetic mechanisms.^{2,14-22} Nonetheless, recent data suggest that non-neuronal actors (i.e., glial cells as well as immune cells in the nerve tissue and in the skin) are also involved in neurotoxicity and neuropathic pain development, highlighting the urgent need to overcome the "neurocentric" view of CIPN (^{23-27,28-30}). Moreover, accumulating research hints to a potential involvement of the vascular compartment in the pathophysiology of neuropathies^{25,31-34} and, since this could envisage relevant therapeutics, an appropriate investigation is mandatory.

In this work, we investigated *ex vivo* the alterations induced by two common neurotoxic chemotherapy drugs (PTX and cisplatin) on the vascular component of the "neuro-glial-vascular unit" in both the somatosensory CNS and PNS. Here, we explore modifications in the

angiogenesis in the CNS and PNS of rats affected by CIPN by using synchrotron radiation-based X-ray phase-contrast micro-tomography (XPCT) from *ex vivo* samples. The results shed light on new pathogenic mechanisms and potential novel molecular targets for future therapeutic approaches for painful-CIPN.

2 | MATERIALS AND METHODS

2.1 | Animals

Forty-eight female Wistar rats (175–200 g upon arrival) were purchased from Envigo Laboratory (Udine, Italy). The age, sex and strain were chosen based on previous studies that demonstrated the appropriateness of the animal models.^{16,20,26} The animals were housed under a 12-h light/dark cycle in the animal facility-controlled rooms (maintained at $22 \pm 2^\circ\text{C}$ with a relative humidity of $55 \pm 10\%$) with *ad libitum* access to food and water. Their clinical conditions were monitored daily, and the weight changes were recorded once or twice a week for drug dose adjustment. All experimental procedures were conducted in conformity with the institutional guidelines in compliance with national (D. L.vo 26/2014, Gazzetta Ufficiale della Repubblica Italiana, n.61, 14 March 2014) and international laws and policies (European Union directive 2010/63/UE; Guide for the Care and Use of Laboratory Animals, U.S. National Research Council, 8th Ed. 2011). The study procedures were authorised by the Italian Ministry of Health (authorisation number 1161/2016). Throughout the duration of the study, the rats were monitored daily for evidence of debilitation due to drug treatments (i.e., piloerection, kyphosis, mucosal dehydration, rhinorrhoea, decreased grooming, eating and drinking, decreased exploring and nesting). Any animal showing obvious signs of suffering or losing more than 20% of its body weight from the beginning of the study would be euthanised.

2.2 | Drugs

PTX (powder, LC Laboratories, Woburn, MA, USA) was prepared as previously reported in the study by Pozzi et al.²⁶ and injected intravenously (i.v.) at the dose of 10 mg/kg, 1 mL/kg. Cisplatin (CDDP; 1 mg/mL solution, Accord Healthcare Limited, Middlesex, UK) was injected intraperitoneal (i.p.) at the dose of 2 mg/kg, 1 mL/kg, in saline solution.

2.3 | Transcardiac perfusion for microvessels labelling and tissue preservation

Transcardiac perfusion was performed as reported previously.³⁴ Saline solution, followed by 4% paraformaldehyde and Indian ink (Rohrer and Klingner KG, Zella-Mehlis, Germany) were employed to label the vascular network and perform the analysis of the microvasculature in the CNS and PNS. More in detail, after anaesthesia, the perfusion was performed using peristaltic pumps (Heidolph Pumpdrive 5101,

Biosigma, Cona, Venice, Italy) as follows: 200 mL/rat of saline solution was employed to clean the vessels from the blood. Immediately after, 200 mL/rat of 4% paraformaldehyde was infused to effectively fix and preserve the tissues. Finally, 200 mL/rat of Indian ink was used to mark the vasculature. The same procedure, without the use of Indian ink, was conducted on the animals destined for morphological investigations and immunolocalisation.

2.4 | Experimental design

Forty-eight rats were randomised into four groups of 12 animals each. Twelve rats were treated with PTX 10 mg/kg, i.v. in the tail vein (PTX-drug), once a week for 4 weeks (cumulative dose 40 mg/kg) and 12 rats were injected with CDDP 2 mg/kg, i.p., twice a week for 4 weeks (cumulative dose 16 mg/kg, CDDP-drug). The remaining 24 animals were divided into two groups of 12 animals each and treated with the respective vehicles' solutions (PTX-Vehicle/10% tween 80, 10% EtOH absolute in saline solution and CDDP-vehicle/saline solution). All the animals in the study underwent neurophysiological and neuropathic pain assessments. At baseline and at the end of the drug treatments, neurophysiological analyses were performed to assess the functionality of peripheral nerves while neuropathic pain was evaluated through behavioural tests for the mechanical and thermal thresholds. An appropriate randomisation of the animals was performed after baseline measurements, to obtain homogeneous groups before starting the drug treatments. After *in vivo* evaluations, 3 days after the last drug injection, animals were perfused and/or sacrificed and employed for tissue collection. Four animals/group were transcardially perfused with Indian ink and paraformaldehyde 4% and used to collect L4-L5 dorsal root ganglia (DRG), L4-L5 spinal cord and S1 brain cortex for the XPCT analysis. Four animals/group were perfused only with 4% paraformaldehyde and employed to collect peripheral nerves (sciatic and caudal) and L4-L5 DRG for qualitative and quantitative evaluations at light microscopes or for immunofluorescence analysis. Finally, four animals/group were euthanised by CO₂ inhalation followed by cervical dislocation and employed to sample the skin biopsies for the quantification of the intra-epidermal nerve fibre (IENF) density. For a summary of randomisation and analysis planned, see Table 1. In full respect of the Reduction principle of the 3Rs, the number of animals/group ($n = 12$) was selected to obtain reliable results and enough biological samples to perform the analysis planned in this paper and in other experiments ongoing at the Experimental Neurology Unit of the University of Milano-Bicocca (see statistics). Conserved blinded operators performed all the analyses planned in this study.

2.5 | In vivo evaluation of peripheral neurotoxicity: nerve conduction studies

Neurophysiological assessments were performed at baseline, and 3 days after the completion of the chemotherapy treatments, using

TABLE 1 Experimental design.

Groups	In vivo analysis	XPCT analysis	Morphological, morphometrical analysis on peripheral nerves and DRG, IF analysis	IENF density
PTX-vehicle	12	4 ^a	4 ^a	4
PTX-drug	12	4 ^a	4 ^a	4
CDDP-vehicle	12	4 ^a	4 ^a	4
CDDP-drug	12	4 ^a	4 ^a	4

Note: The table shows a summary of the number of animals employed for each group, the treatments and the analysis performed in the study. Abbreviations: CDDP, cis-diamine-dichloroplatin; IF, immunofluorescence; PTX, paclitaxel; XPCT, X-ray phase-contrast tomography.

^aAnimals perfused.

the Matrix Light electromyography apparatus (Micromed, Mogliano Veneto, Italy), as previously described.³⁵ Sensory nerve conduction velocity (SNCV) and amplitude of the sensory nerve action potential (SNAP) for both proximal caudal and digital nerves were obtained, keeping animals under deep anaesthesia with isoflurane and controlling body temperature with a thermal pad controlled via a rectal probe.

2.6 | In vivo evaluation of neuropathic pain: behavioural tests

Dynamic Plantar Aesthesiometer and Plantar tests were performed to explore the mechanical and thermal thresholds of the animals, at baseline and 2 days after the completion of the chemotherapy regimens. Paw withdrawal threshold in response to mechanical stimulus was assessed using a Dynamic Plantar Aesthesiometer apparatus (Ugo Basile Biological Instruments, Varese, Italy) as reported in the study by Pozzi et al.²⁶ The response to the non-nociceptive mechanical stimulation was registered three times for each paw and then calculated as the average of six repeated trials (expressed in grammes).

The paw withdrawal threshold in response to infrared heat stimulus was assessed using a Plantar instrument (Ugo Basile Biological Instruments) as previously described in the study by Meregalli et al.³⁶ The time of hind paw withdrawal was recorded three times for each paw and then calculated as the average of four repeated trials (expressed in seconds). For both mechanical and thermal tests, cut-offs were fixed to avoid paw damage.

2.7 | Anaesthesia and euthanasia

For neurophysiology, anaesthesia was induced in a chamber with 3% isoflurane carried in oxygen followed by 3%–3.5% isoflurane in the nose cone for maintenance during the procedures. The corneal blink response and any withdrawal physical response to external stimuli were adequately suppressed. To avoid isoflurane-induced hypothermia, the body temperature was maintained at $37.0 \pm 0.5^\circ\text{C}$ using a heating pad (Homoeothermic System, Harvard Apparatus, Holliston, MA, USA).

At the end of the experiments, before sample collection, the animals were anaesthetised with Ketamine/Xylazine (Lobotor

100 80 mg/kg/Xilazina 2% 10 mg/kg) for the transcardiac perfusion or euthanised by CO₂ inhalation followed by cervical dislocation.

2.8 | Structural characterisation of peripheral neuropathy

2.8.1 | Neuropathological analysis

For morpho-structural investigations, sciatic, distal caudal nerves (approximately 5 cm from the base of the tail extremity, the point of neurophysiological recordings) and L4-L6 DRG from four perfused animals/group were collected and processed as described in the studies by Meregalli et al. and Pozzi et al.^{22,26} for light microscopy observations and quantitative analysis (see paragraph below). Semithin sections of 1.5 μm-thickness were prepared and stained with toluidine blue. Finally, the obtained sections were examined and representative images were taken with a Nexcope Ne920 AUTO light microscope (TiEsseLab Srl, Milano, Italy).

2.8.2 | Morphometrical analysis of DRG

Serial 1.5 μm sections, spaced of 50 μm, were prepared for the morphometric analysis of L4-L6 DRG as reported in (Meijer et al., 1999)³⁷ with adjustments. Briefly, stitching images of DRG sections were captured with a light microscope-incorporated camera (Nexcope Ne920 AUTO light microscope, TiEsseLab Srl, Milano, Italy) at a magnification of 20×. The somatic, nuclear and nucleolar sizes of at least 200 DRG neurons/rat were manually measured from three animals/group and analysed with a computer-assisted image analyser (ImageJ software, US National Institutes of Health).

2.8.3 | Intra-epidermal nerve fibre density

To evaluate the damage of small unmyelinated peripheral nerve fibres, a parameter correlated with both neurotoxicity and neuropathic pain induced by chemotherapy, the IENF density in the hind paw footpad of three non-perfused animals/group was measured as described before.³⁸ Plantar glabrous skin biopsies (5 mm) from the right hind paws were

fixed in 2% paraformaldehyde-lysine-sodium periodate solution for 24 h at 4°C and cryoprotected at -20°C until use. Samples were then serially cut into 20 µm sections with a cryostat. Free-floating immunohistochemistry was performed on six randomly selected sections from each footpad on a 96-well tissue culture plate under a stereomicroscope. After blocking in 4% of NGS + 0.1% of triton X-100, sections were incubated in rabbit polyclonal antibody anti-protein gene product 9.5 (Proteintech Europe, Manchester, UK). After rinses, sections were exposed to the anti-rabbit biotinylated secondary antibody (Vector Laboratories Newark, CA, USA). Sections were then incubated with Vector ABC, avidin-biotin mix from Vectastain ABC-HRP kit (Vector Laboratories Newark) and finally, in the blue chromogen/peroxidase substrate (Vector SG-HRP substrate kit, Vector Laboratories Newark) until the reaction was completed. The total number of nerve fibres that cross the dermal/epidermal junction was counted from three sections/animal under light microscopy at high magnification, the length of the epidermis was manually measured (Image J software, US National Institutes of Health) and the linear density of IENF/mm was obtained.

2.8.4 | X-ray phase contrast tomography analysis of vascular network

The experimental framework used to reconstruct the 3D vessel microstructure in the nervous is illustrated in Figure 1. Samples were housed in Teflon tubes sized 1.2–2.4 mm in diameter, 1 cm long and subsequently acquired at the synchrotron facility. The cylinder-shaped samples were collected from three different regions of the nervous system:

L4-L5 DRG, L4-L5 spinal cord at L4-L5 and the primary somatosensory cortex (S1). For the S1 samples, we directly cored the right parietal lobe of the extracted brains by gently rotating and inserting the Teflon tube (1.2 mm in diameter) orthogonal to the cortical surface. Lumbar spinal cords and DRGs were first extracted and then gently inserted in the 2.4 mm thick tubes. Tubes were closed both at the top and the bottom ends with a tip of semi-liquid paraffin pre-heated at 45°C.

XPCT studies were carried out at SYRMEP (Synchrotron Radiation for MEical Physics) beamline of Elettra Sincrotrone Trieste S.C.p.A (Italy) using the available high-resolution white/pink beam setup.³⁹ The CT scans were performed with an average energy of 19.3 keV by filtering the energy spectrum with a 1 mm Si filter. The samples were imaged in free space propagation mode setting a sample-to-detector distance of 12 cm. Raw images were acquired using an sCMOS camera (Hamamatsu Orca Flash 4.0, 2048 pixels × 2048 pixels having a physical pixel size of 6.5 µm × 6.5 µm) coupled to a 17 µm thick GGG scintillator screen. Thanks to an optical magnification system, the effective isotropic pixel size was 0.9 µm yielding a field of view of about 1.8 mm × 1.8 mm. XPCT scans were acquired by collecting 1800 projections (equally spaced) over 180° with an exposure time of 200 ms per radiography. The acquired datasets also comprised 20 flat fields (i.e., images of the brunbackground) and 20 dark images. The tomographic reconstructions were performed using the open-source software SYRMEP Tomo Project (STP, v.1.6).⁴⁰ Projections were first pre-processed through conventional flat fielding method and potential ring artefacts were attenuated by applying a Rivers filter with width 11. Projections were phase retrieved using Paganin's algorithm with a delta/beta ratio equals to

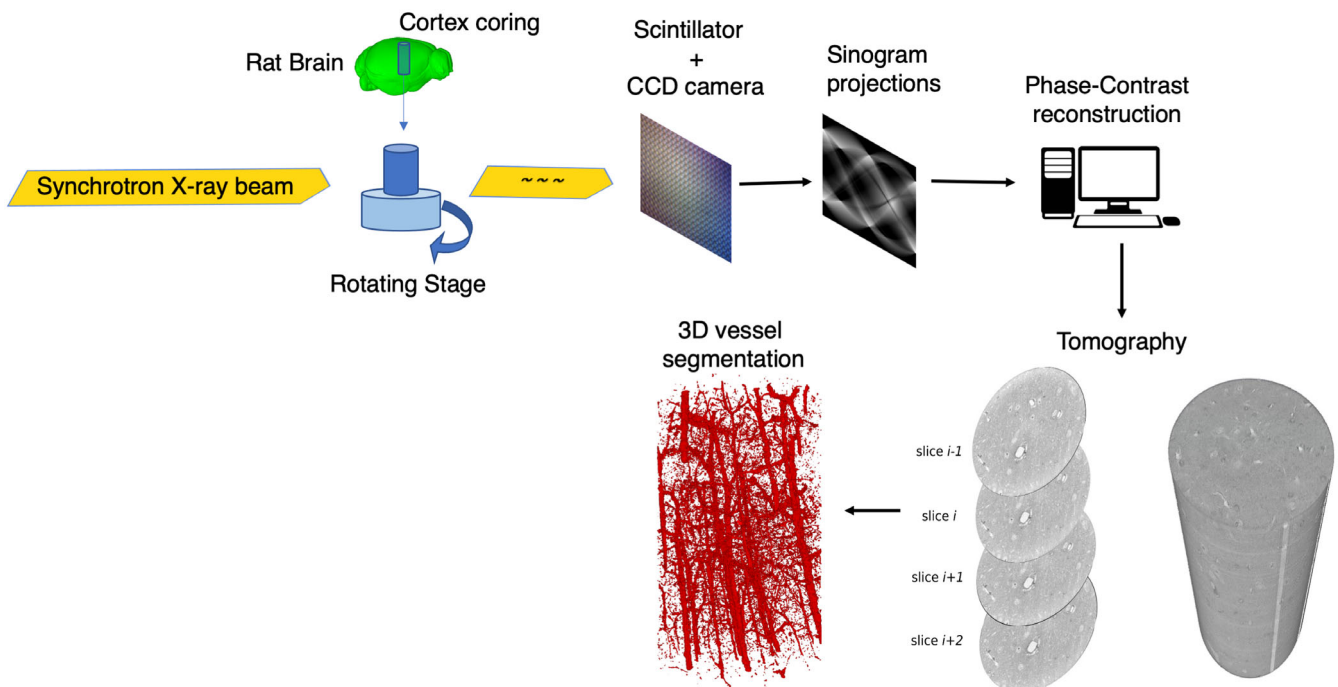


FIGURE 1 The experimental framework used to reconstruct the 3D vessel microstructure from the cortical coring. The synchrotron-generated X-ray beam hit the cortical sample held on a rotating stage. The exiting beam excites a scintillator and the emitted visible light is collected by a digital camera sensor. Resulting projections are processed by a computer that reconstructs the 3D microCTs slice-by-slice. At last, an automatic segmentation algorithm extracts the entire 3D vascularisation of the scanned brain tissue sample.

4 and finally, virtual slices were obtained by applying Filtered Back Projection algorithm combined with a Shepp-Logan filter.

2.9 | Computational analysis

The scope of the imaging technique was to extract vessels from the virtual slices returned by the XPCT studies, an operation commonly named *segmentation*. For this purpose, we tuned a computational processing pipeline as follows. Reconstructed volumes were first converted to 8-bit from the original 32-bit tiff format and then the Frangi vesselness filter was applied by using the *fibermetric* Matlab built-in function. Afterward, obtained volumes were automatically thresholded in ImageJ by using the Shanbhag method. At the end of that step, the binarised volume usually contained a small fraction of false positive vessels to be removed. They typically belong to spurious radiodense neuron somas or regions at the sample borders. In order to eliminate those structures, we used a connected component filtering implemented by the MorphoLibJ Fiji plugin. More in detail, we first computed the 3D connected component labelling with an Euler connectivity parameter of 26. That operation returned clusters of contiguous 3D voxels that were individually characterised by counting the number of constituent voxels. Clusters that had fewer than 40 voxels were discarded because they putatively represented neuron somas. By a visual inspection, we removed clusters dispersed over the sample borders. At the end of the segmentation process, volumes represented vessels by 1's over 0's (no vessels) and were analysed to estimate important vascular features like the density, the diameter, the branching factor and the tortuosity. An estimate of the vascular density was computed by the ratio between the number of vascular voxels over the number of total voxels (Figure 2A). The estimation of the diameter for each vessel segment was done by computing the largest inscribable equivalent ellipsoid and averaging the two smallest ellipsoid axes (Figure 2B). Further characterisations of the vascular network required a skeletonisation that transformed each vessel segment into diameterless cylinders using the built-in ImageJ 3D skeletonisation function (Figure 2C). In this way, we estimated the bifurcation points (sites where a single vessel gives birth to another or more vessels) and the tortuosity (the extent of the curviness of the vessel segment, Figure 2D).

2.10 | Immunofluorescence analysis for microvasculature in the S1 cortex, L4-L5 spinal cord, DRG

To histologically visualise the blood vessels and corroborate the quantitative results obtained by XPCT, L4-L6 DRG, L4-L5 spinal cord and S1 cortex of four perfused animals per group were dissected, post-fixed in 10% formalin for 3 h at RT, infiltrated with a 30% sucrose solution and frozen. Ten-micrometre-thick serial slices were then cut with a cryostat and incubated with Lectin from *Lycopersicon Esculentum* (tomato) in PBS (1:1000, Sigma-Aldrich, USA), washed in PBS, mounted and analysed on a confocal microscope

(LSM710, Zeiss, Germany). Negative controls were incubated in PBS.

2.11 | Statistical analysis and G-power

The sample size, as the number of animals/group to be employed, was determined by considering the power analysis and the biological sample demand. In respect of the “reduction” principle of the 3Rs, the biological samples harvested were employed for morphological and molecular analysis described before in this study and for other experimental research performed at the Experimental Neurology Unit of the University of Milano-Bicocca. The estimate of the sample size per group has been calculated on the basis of the main objective of the study: the development of alterations in the mechanical threshold. Assuming the biologically meaningful difference between chemotherapy-treated animals versus vehicles of 5 g (i.e., a variation of around 20%–30%) with an alpha value of 5% and a power of 80%, the required number of rats would be a minimum of eight/group. The number of animals employed was definitely 12/group, in order to satisfy the biological sampling demand. Data deriving from nerve conduction studies were analysed with unpaired *t* test with Welch's correction. Data from behavioural tests, IENF density, were analysed with multiple non-parametric *t* tests (Mann–Whitney test, Bonferroni post-hoc test for multiple comparisons). DRG morphometry was analysed with non-parametric *t* tests. Results from 3D reconstructed vascular networks were obtained by analysis of variance (ANOVA) one-way comparisons with Tukey's post-hoc test for multiple comparisons. Second level analyses comparing nervous system regions were modelled by a two-way ANOVA test with Tukey's post-hoc test for multiple comparisons. We performed multiple comparisons just for the contrasts: for neurophysiological analysis, behavioural test, XPCT analysis: PTX-vehicle versus PTX-drug and CDDP-vehicle versus CDDP-drug; for the effect size of XPCT analysis among regions: CDDP versus PTX. A *p*-value <.05 was set as significant. All analyses were conducted with GraphPad prism software (v 9.0).

3 | RESULTS

3.1 | In vivo assessments of chemotherapy-induced peripheral neurotoxicity and neuropathic pain

At baseline, sensory nerve conduction studies (SNCV, Figure 3), together with behavioural testing, were used to ensure proper randomisation of the animals and groups homogeneity (data not shown). The results of the in vivo analyses performed to assess the neurotoxic effects of PTX and CDDP at the end of the treatments are reported in Figure 3. SNCS were used as parameters to verify if axonal damage had ensued in peripheral (caudal and digital) nerves. The behavioural tests were performed to assess the mechanical and the thermal thresholds of the animals, as parameters indicating the establishment of neuropathic pain. At the end of the treatments, a significant decrease in caudal and digital SNAPs together with a reduction of caudal nerve conduction

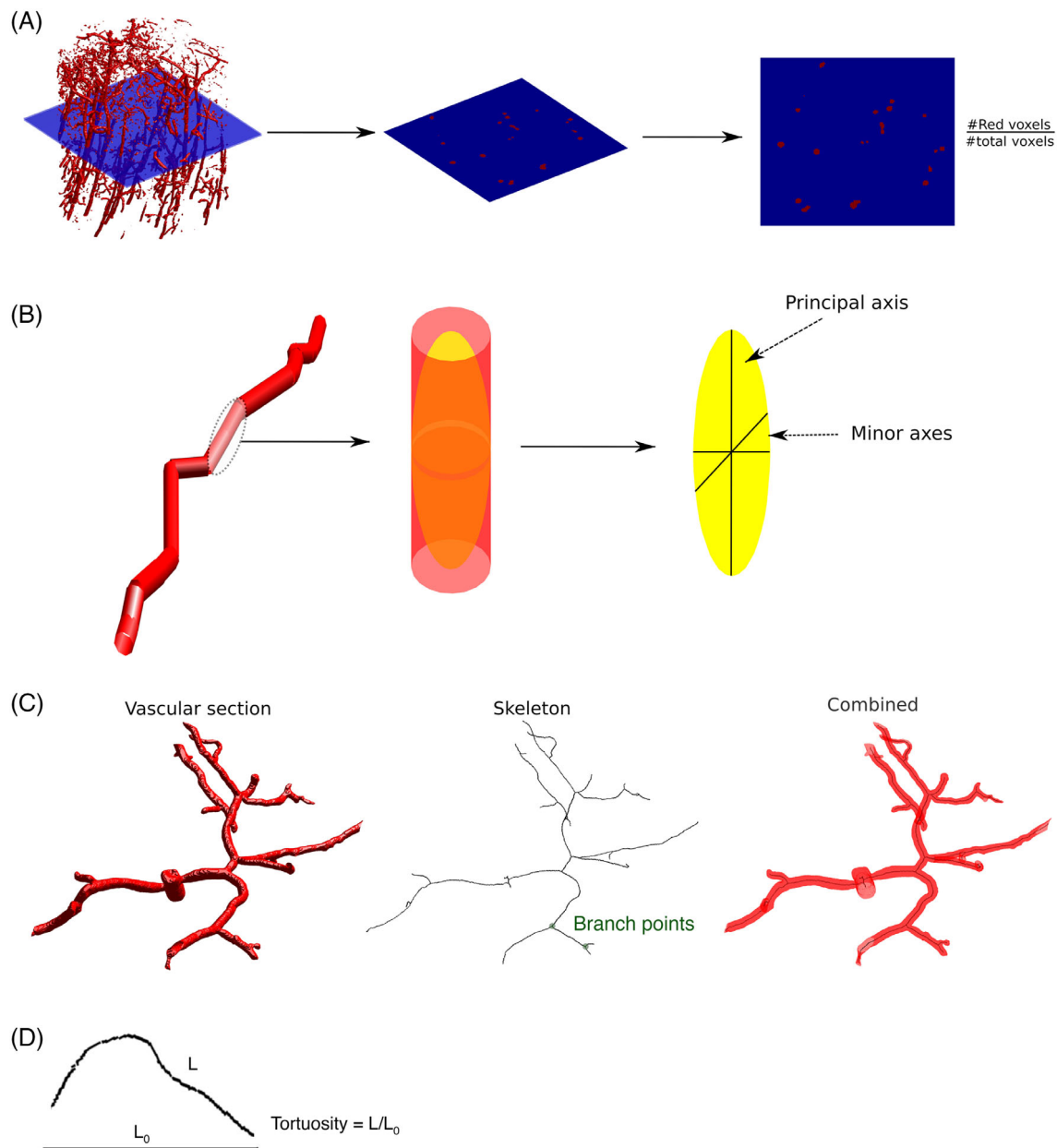


FIGURE 2 Estimation of the vascular network metrics. (A) Vascular density is simply obtained as the ratio between the number of voxels indicated as “vessels” by the segmentation algorithm and the number of total voxels. (B) Ellipsoids inscribed in each vascular segment approximate the vascular diameter by averaging the two minor axes. (C) The entire vascular network is skeletonised by reducing the diameter of each segment to just one point. This operation allows for the estimation of topological measures like the length density and the tortuosity (D).

velocity were recorded in PTX-treated animals compared to their vehicles, indicating the establishment of a sensory axonal polyneuropathy (data in Table S1). CDDP treatment determined a mild, but significant, decrease in the caudal amplitude of nerve potential. As expected, mechanical allodynia and thermal hypoalgesia (Figure 3), intended as an increased sensitivity for non-nociceptive mechanical stimulations and a decrease in sensitivity to thermal stimulation, were evident at the end of the treatment with PTX (data in Table S1). No alterations in mechanical and thermal thresholds for animals treated with CDDP were recorded. These data, as expected, suggested the development of neuropathic pain in animals treated with PTX.

3.2 | Neuropathological study of chemotherapy-induced neurotoxicity

3.2.1 | Peripheral nerves and intra-epidermal nerve fibres

Representative sections of caudal nerves and skin biopsies of animals treated with PTX, CDDP and vehicles are reported in Figure 4, as well as quantitative results of morphometrical investigations on skin epidermis.

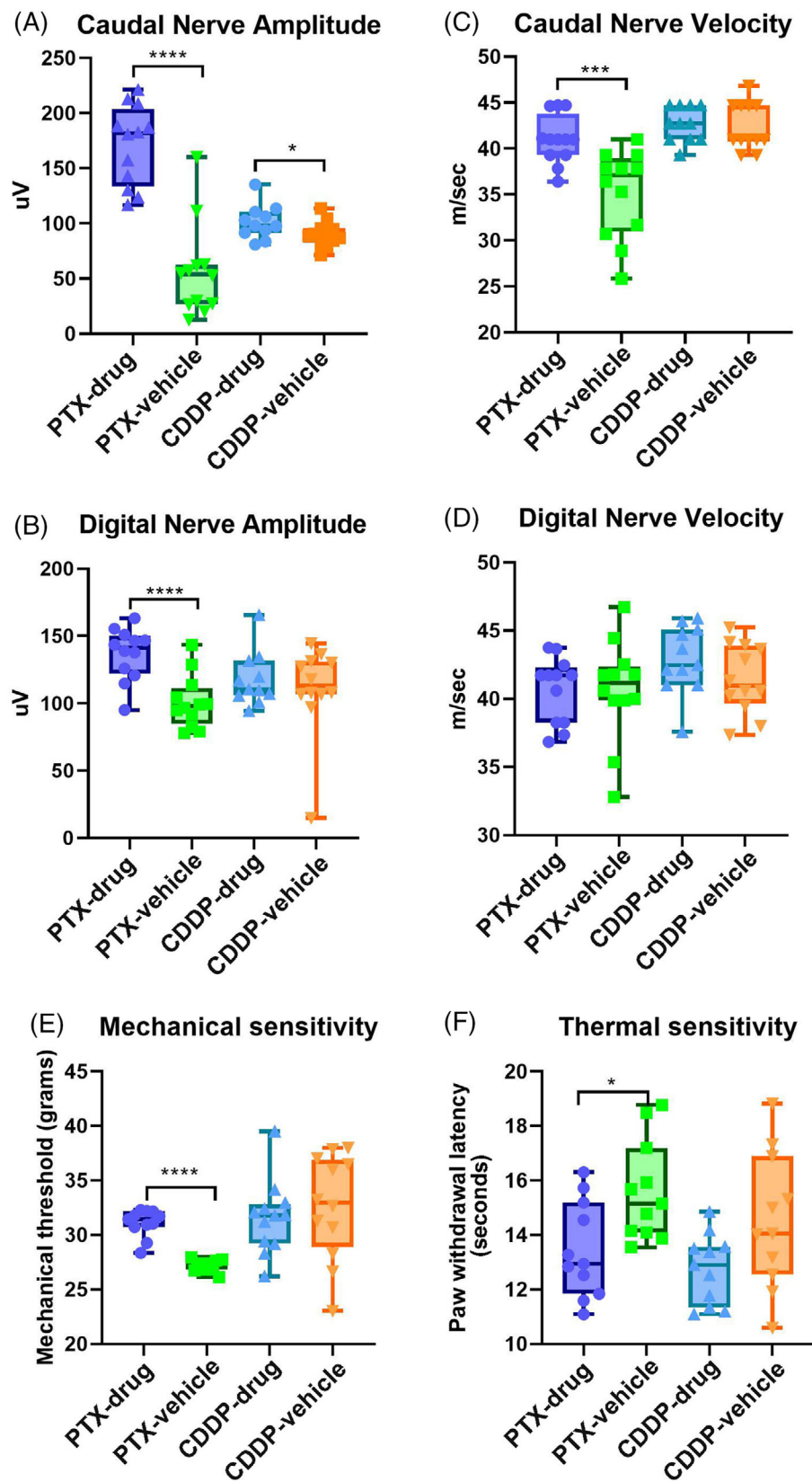


FIGURE 3 Nerve conduction studies for the functionality of nerves and behavioural tests for the neuropathic pain. Twelve animals/group were tested at baseline (not shown) and at the end of chemotherapy treatments for the functional analysis of the peripheral nerves measuring the caudal and digital nerve potential amplitudes (A and B) and caudal and digital nerve conduction velocities (C and D) and for the mechanical and thermal thresholds (as measures of the development of neuropathic pain) by dynamic tests (E) and plantar test (F) (CDDP, cis-diamine-dichloroplatin; IR, Infrared intensity; PTX, paclitaxel) (p -value significance: * $p < .05$; ** $p < .01$; *** $p < .001$; **** $p < .0001$; Mann-Whitney U test).

Morphological examination of caudal nerves, harvested after sacrifice at the end of treatment with PTX confirmed the development of axonopathy: as reported in Figure 4A, an overall degeneration of

myelinated fibres as well as a severe loss of fibres were evident in PTX-drug compared to PTX-vehicle that could justify the statistically significant impaired neurophysiology (Figure 3A-D). The same

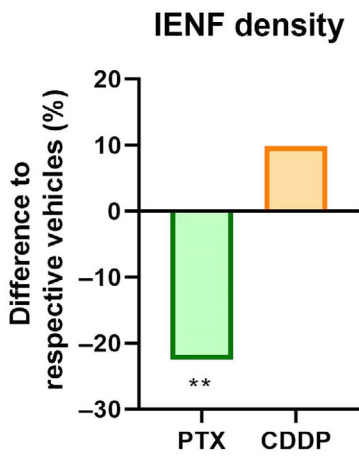
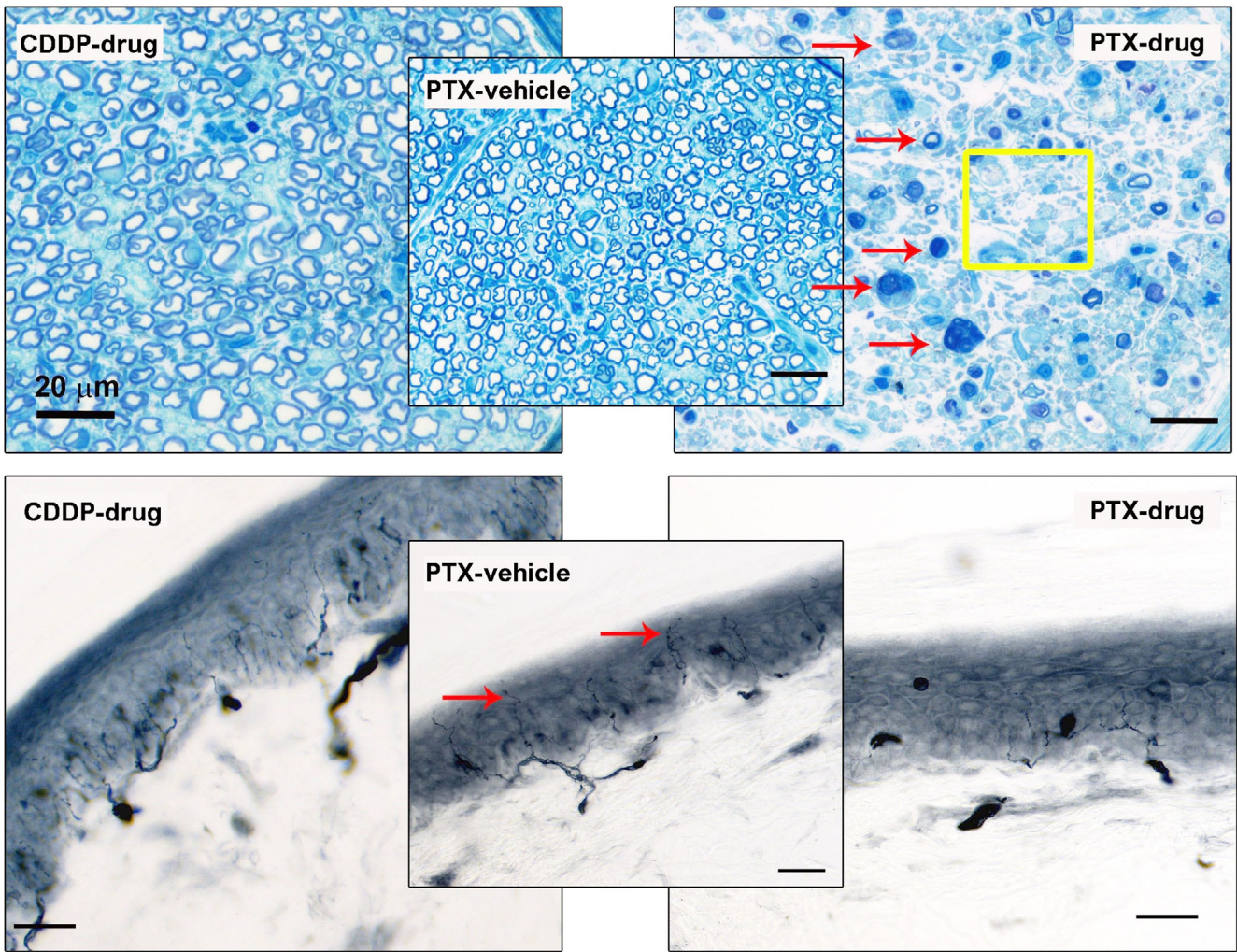


FIGURE 4 Legend on next page.

FIGURE 4 Morphological and morphometrical studies on caudal nerve and skin biopsy. Representative images of caudal nerves (A) and skin biopsies (B) are reported. Nerves and skin from four animals/group were analysed. Degenerated myelinated fibres are indicated by way of examples by red arrows in (A) whereas the extensive areas of myelinated fibre loss (as an indication see the yellow square in (A)). Intraepidermal unmyelinated fibres are indicated by way of examples by red arrows in (B). A massive loss of these fibres is evident in PTX-treated animals. C represents the quantitative analysis of IENF (% rate change): PTX, but not CDDP, induced a significant loss of small unmyelinated fibres in the epidermis (IENF, intraepidermal nerve fibres; CDDP, cis-diamine-dichloroplatin; PTX, paclitaxel; bar = 20 μm) (p -value significance: * $p < .05$; ** $p < .01$; *** $p < .001$; **** $p < .0001$; Mann-Whitney U test).

analysis performed on CDDP specimens indicated no relevant structural abnormalities in the myelinated fibres at light microscope. However, as previously reported,²⁶ the morphometrical analysis of caudal nerve revealed a slight decrease in the frequency of large fibres in CDDP (data not reported). This suggests, since no alterations in the global fibre density were observed, an increased rate of smaller-caliper fibres versus larger ones. Caudal nerves of PTX-treated animals resulted in being too damaged to perform the morphometrical analysis.

The qualitative observation and a quantitative analysis of small unmyelinated fibres in the skin biopsy (Figure 4B,C and Table S2) revealed a significant decrease in the IENF density for PTX animals compared to vehicles. On the other hand, no changes in the small unmyelinated fibres were detected in CDDP-treated animals.

3.2.2 | DRG

As a confirmation of the data previously published,²⁶ the morphological examination of L4-L6 DRG at light microscope did not reveal any obvious alterations in the cyto-preservation of sensory neurons in PTX animals (data not shown). The analysis of DRG from CDDP-treated animals demonstrated, as expected, the development of a peripheral neuropathy: some structural changes in the DRG sensory neurons, that is, nucleolar eccentricity and increased number of nucleoli evidenced by arrows and arrowheads respectively, were present in CDDP-drug compared to CDDP-vehicle (Figure 5). These observations were enriched by morphometrical examinations (Figure 5A-C) that evidenced a statistically significant atrophy of DRG neurons (Table S3).

3.3 | Morphological and topological characterisation of the reconstructed vascular systems

Three-dimensional volumes obtained from XPCT reconstructions were processed according to a computational pipeline to filter artefacts and noise and to segment vascular objects from the rest of the cellular substrate (see Section 2). Differential analyses among groups (PTX-drug vs. PTX-vehicle and CDDP-drug vs. CDDP-vehicle) were performed on four vascular system measurements: the vascular density (the percentage of vessel volume over the total volume), the vessel diameter (the distribution of the estimated vessel diameters), the tortuosity (the estimation of the curvature of each vessel) and

the number of branch points (the number of points where vessels bifurcate giving birth to another vessel).

The results of this analysis are reported in Figure 6 and Table S4. Vascular density largely varied among groups in the explored nervous system regions. The DRG had significantly higher vascular density in PTX rats compared with its vehicle. A similar result was found also in the lumbar tract of the spinal cord (L4-L5) and in S1 (Figure 6A and Table S4). In contrast, vessels had significantly thinner diameters (Figure 6B and Table S4) in the PTX group compared to vehicle group in all three regions. This finding suggests that novel vessels were probably constituted by smaller capillaries, which cause the average diameter to collapse.

In the second part of the analysis, the reconstructed vascular architectures were skeletonised, an operation that transforms vessels into topological objects described by just segments and bifurcation points. During vasculogenesis and angiogenesis, a vessel segment commonly bifurcates, leading to another vascular segment. By analysing the number of bifurcations (branch points), we found a significant increment in the PTX group compared to the vehicle (in L4-L5 spinal cord and in S1). From this perspective, we analysed the tortuosity, that is, how much a vascular segment tends to be a straight line or, conversely, a circular shape. Moreover, we found that vessels from the PTX group were less tortuous, namely, they were more prone to be straight compared to the other groups in the three regions. Altogether, these results confirmed the presence of a conspicuous angiogenesis in the PTX nerve tissues, with alterations in the vascular organisation. In CDDP, the vascular changes were obviously less significant with only an increased complexity in the vessels network (i.e., increased branch points) in S1 (Figure 6C and Table S4), but no alterations in the vascular density and vessel diameter were observed after CDDP treatment.

A qualitative comparison of the extent of the angiogenesis in the different regions of the CNS and PNS in PTX and CDDP animals compared to their vehicles is reported in Figure 7 and in the 3D rendering videos (see Movies S1-S12). The angiogenesis is higher in DRG, spinal cord and S1 of PTX-treated animals compared to the PTX-vehicle. No relevant changes were observable in DRG, spinal cord and S1 of CDDP-treated animals compared to the CDDP-vehicle (Figure 7A-F, J-L and Movies S1-S12).

Eventually, we considered the hypothesis that effect sizes among regions were different and thus we compared each measure among the three nervous system sites over the treatments PTX, CDDP (Figure 8 and Table S5). We found that vascular density was the highest in the PTX-treated S1 (Figure 8A), followed by the lumbar

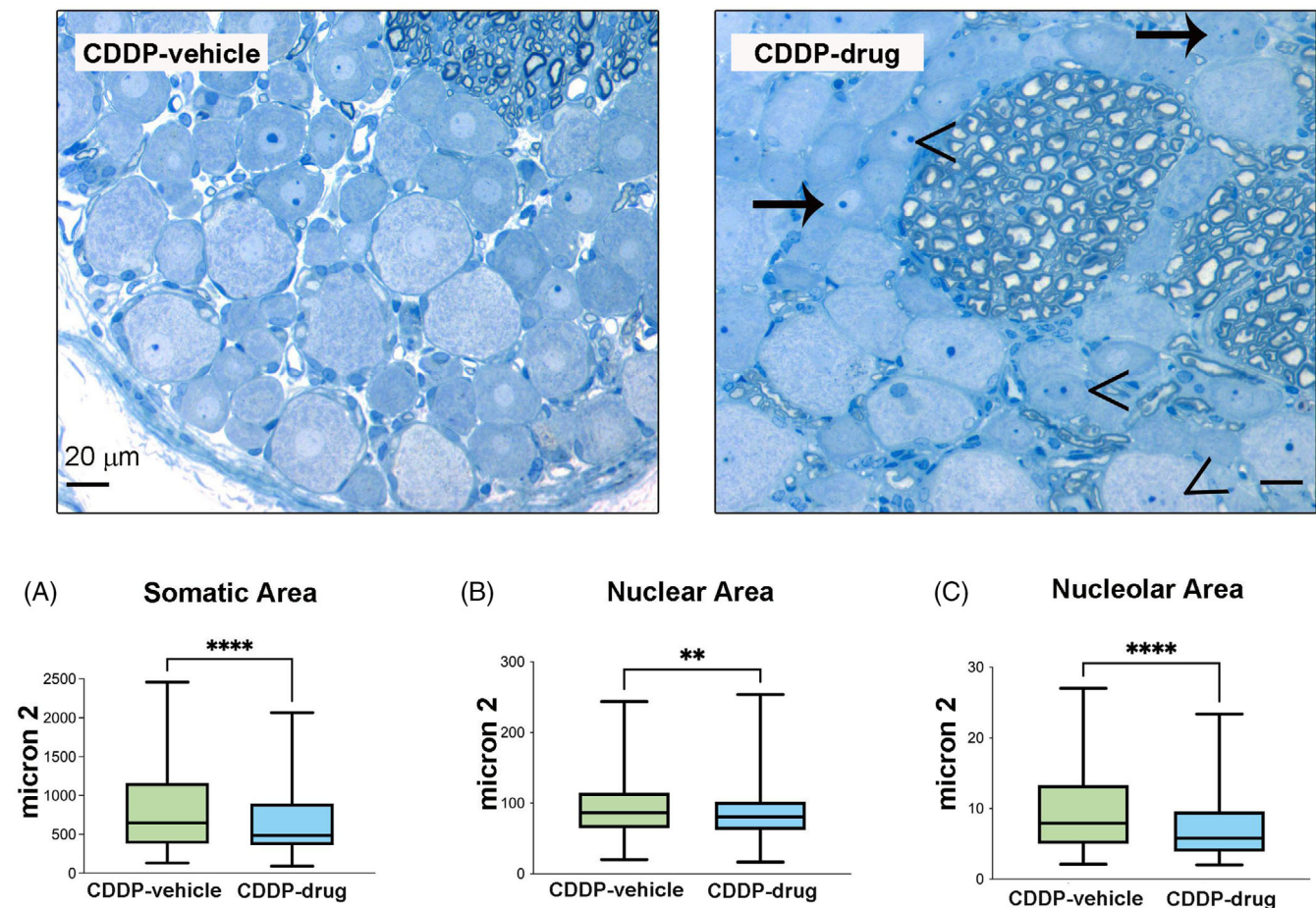


FIGURE 5 Morphological and morphometrical analysis of DRG. Representative microscopy images of DRG from vehicles and CDDP-treated animals together with morphometrical analysis of DRG (A–C) are reported. DRG from four animals/group were analysed. Nucleolar eccentricity (arrows) and multi nucleoli (arrowheads) were evident in DRG of CDDP-treated animals. Morphometrical analysis (mean \pm SEM) reported somatic (A), nuclear (B) and nucleolar (C) atrophy in DRG of CDDP-treated animals (CDDP, cis-diamine-dichloroplatin; bar = 20 μ m) (p -value significance: * p < .05; ** p < .01; *** p < .001; **** p < .0001; Mann-Whitney U test).

spinal cord and the DRG. Similarly, in the CDDP group, S1 is primarily characterised by a relatively maximal vascular density followed again by the lumbar spinal cord and the DRG. Equivalently, average vascular diameter ranked last in the S1 of the PTX group (Figure 8B) followed by DRG, lumbar spinal cord, as well as for the CDDP group. Also, the number of branch points was the largest in the S1 PTX group, followed by the lumbar spinal cord and the DRG (Figure 8C). A similar trend was observed also for tortuosity (Figure 8D). These results indicated that the major effects of the observed putative angiogenesis were located first in the S1, secondly in the L4-L5 spinal cord and eventually in the DRG, a sequence inversely related to the ascending nociceptive pathway.

3.4 | Immunostaining of blood vessels

Finally, we performed some experimental analyses of immunofluorescence in order to investigate the molecular substrate of the observed neo-angiogenesis and “qualitatively” confirm the quantitative XPCT

data. We chose the lectin from tomato (*Lycopersicon Esculentum*), widely employed as a marker of blood vessels and a valuable tool in studying angiogenesis neovascular development.

The results of the immunofluorescence imaging, represented in Figure 9, confirmed a significantly higher concentration of vessels in the L4-L5 DRG, lumbar spinal cord and S1 of PTX-treated animals compared to their vehicles.

4 | DISCUSSION

In this work, we found that, on our schedules of treatment, the chronic administration of rats with PTX induced severe neurophysiological and neuropathological alterations in the peripheral nerves, mechanical allodynia, thermal hypoalgesia and a decrease in intraepidermal small unmyelinated fibre density, indicating the development of a severe painful peripheral axonopathy. CDDP determined a peripheral neuropathy with mild neurophysiological and neuropathological changes in peripheral nerves, severe DRG neurons' structural

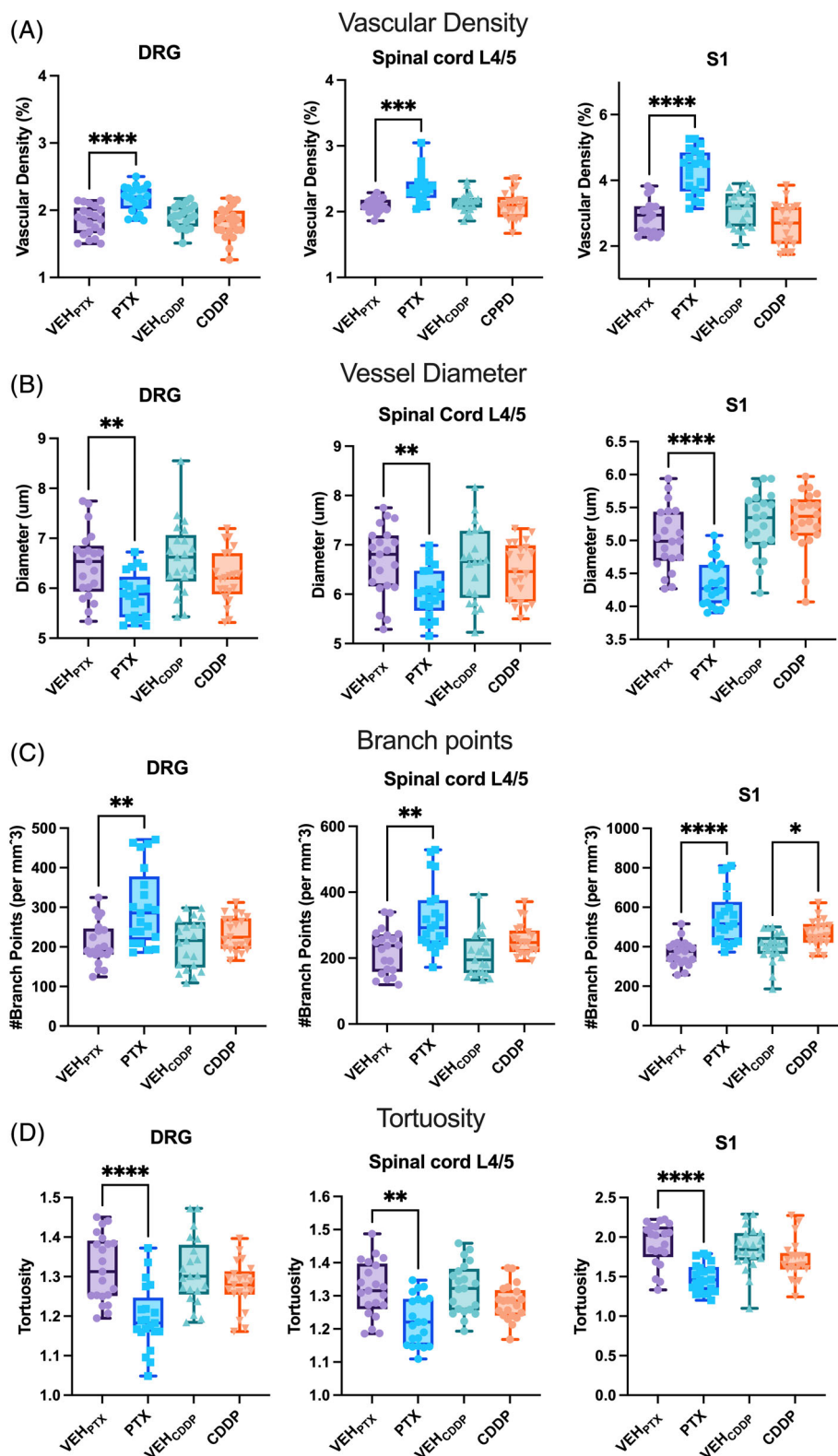


FIGURE 6 Vascular metrics computed on the synchrotron X-ray generated tomographies. Distributions were compared by a one-way ANOVA model over the four experimental conditions (PTX-drug, PTX-vehicle, CDDP-drug and CDDP-vehicle). (A) Vascular density distributions were statistically different in all of three regions (L4-L6 DRG, lumbar spinal cord, S1 cortex; four animals/group were analysed) and post-hoc analyses revealed that in the PTX group, density was significantly larger than the PTX-vehicle group in all of three regions. (B) Vessel diameter distributions were statistically different in all of three regions and post-hoc analyses identified that in the PTX group, average diameter was significantly smaller than the PTX-vehicle group in all of three regions. (C) The distributions of the number of branch points per mm³ were statistically different in all of three regions and post-hoc analyses showed that in the PTX group, there were more branch points than the PTX-vehicle group in all of three regions. (D) Tortuosity was differently distributed over the groups in all three regions and multiple comparison analysis showed that in the PTX group, the tortuosity decreased in comparison to the PTX-vehicle group in all three regions (mean \pm SD; *p*-value significance: **p* < .05; ***p* < .01; ****p* < .001; *****p* < .0001; Tukey post-hoc, *t* test).

alterations and no changes in the sensory thresholds and in small unmyelinated fibre density in the skin. These results demonstrated that, in our animal models of CIPN, the development of neuropathic pain was evident only after PTX, but not CDDP, chronic treatment. These results are consistent with our previous works in which the two

drugs were repeatedly injected for 4 weeks.^{22,26,41} The animal models we employed are, in our vision, optimal to study the pathophysiology of CIPN firstly because they faithfully mimic, in the animals, the prolonged administration schedules of the drugs in humans. Secondly, the chronic injections of the drugs are able to determine, as happened

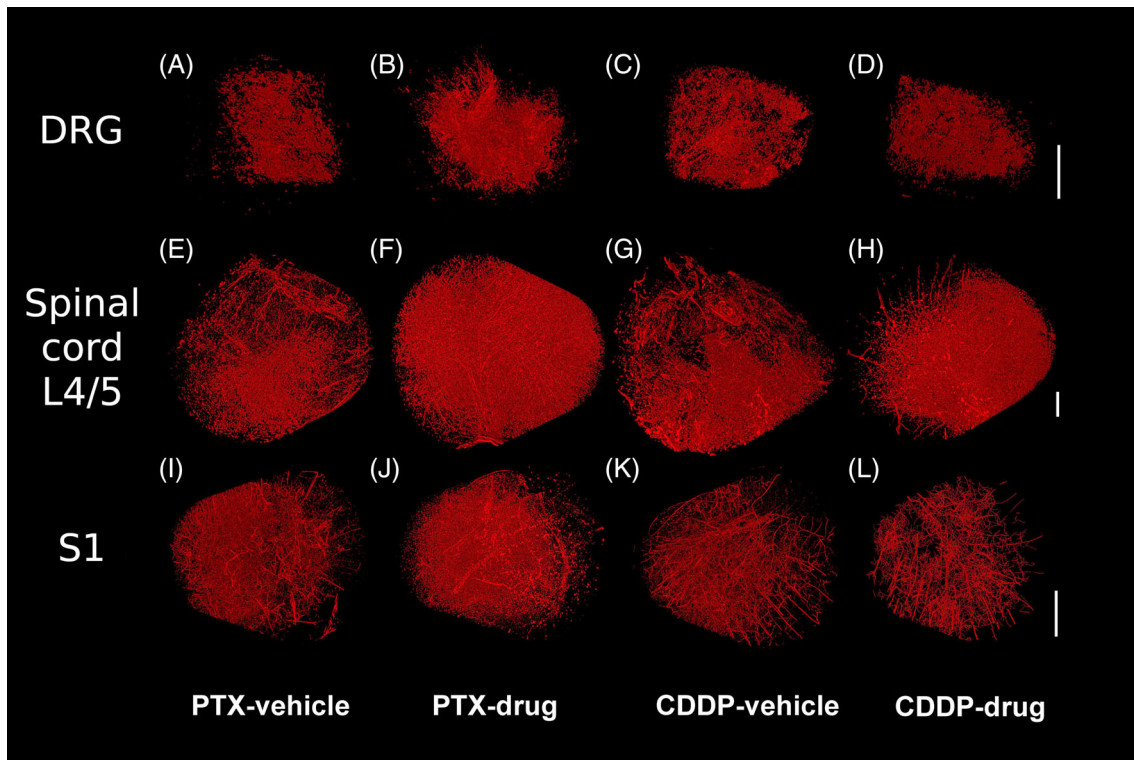


FIGURE 7 Illustrative XPCT tomographies. Vascular network of DRG, lumbar spinal cord and S1 cortex of vehicles and CDDP or PTX-treated animals was obtained by automatic segmentation of the 3D reconstructed XPCT volumes. An evident increment of vascular density was observable only in all the regions of PTX-treated animals (A–D: DRG; E–H: lumbar spinal cord; I–L: S1 cortex; bars [in white]: 500 μm).

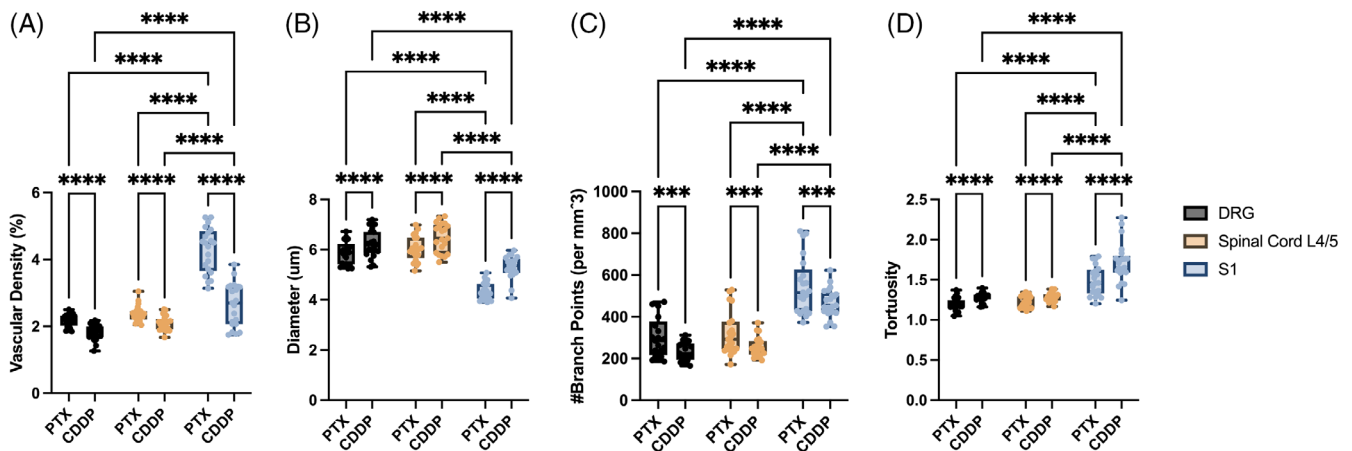


FIGURE 8 Second-level analysis of the angiogenesis measures over the nervous system regions. Measures were compared in two-way ANOVA models by contrasting the treatment (PTX, CDDP) and the region (L4–L6 DRG, lumbar Spinal Cord and S1 cortex). The S1 cortex accounted for most of the expressed angiogenesis in comparison to the other regions in terms of the vascular density (A) and diameter (B). S1 was also the site with the major number of branch points (C) and most tortuous vessel segments (D) (p -value significance: * $p < .05$; ** $p < .01$; *** $p < .001$; **** $p < .0001$; Tukey post-hoc, q test).

in humans, established morphological and functional damage in peripheral nerves and/or in lumbar DRG, as preferential target sites of chemotherapy drugs not protected by the blood–brain barrier. Moreover, the development of pain, if present, is also well established, and is the result of the chronicisation of nerve damage in the PNS. Other works in the past demonstrated the development of transient

alterations of mechanical and thermal thresholds shortly after one single or few repeated injections of CDDP.^{42,43} These altered thresholds are, in these cases, not related to nerve damage since one or few administrations of the drug are not enough to determine chronic nerve damage. For these reasons, the results of these studies are not comparable with those obtained in our study as the administration

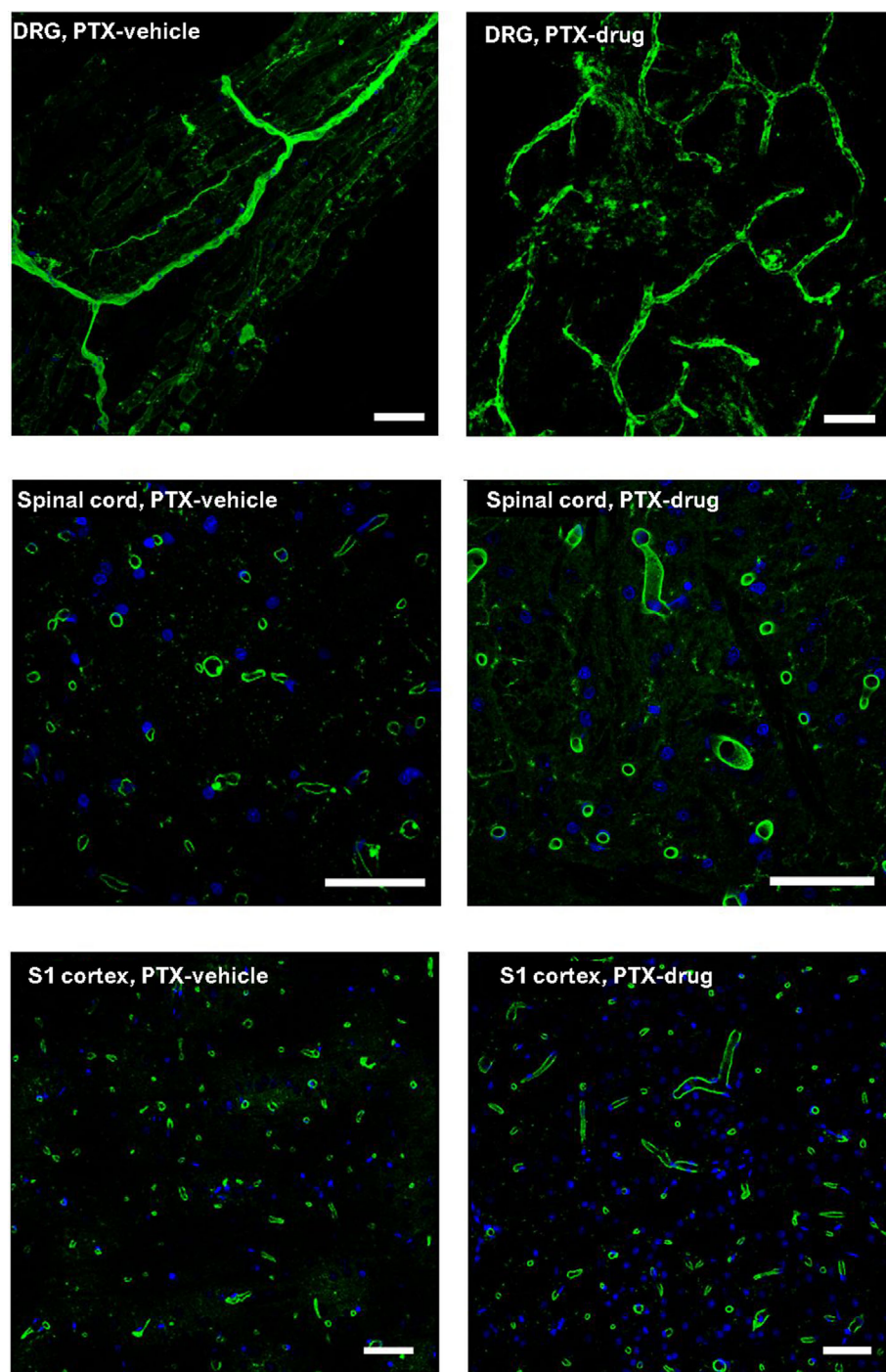


FIGURE 9 Immunofluorescence analysis on DRG, lumbar spinal cord and S1 cortex. Lectin from tomato (green), evidences the wall of blood vessels; DAPI (blue) stains the cell nuclei. The density of blood vessels qualitatively increased in DRG, lumbar spinal cord and S1 cortex of PTX-treated animals compared with respective vehicle-treated animals. Three animals/group were analysed (bar = 50 μ m).

schedule and the threshold evaluation timing were different. Moreover, to support our results, the development of neuropathic pain in patients exposed to CDDP-based chemotherapy is not as common as during other chemotherapy regimens as those based on PTX, oxaliplatin and bortezomib.³ Paraesthesia, progressing to proprioceptive loss, areflexia and sensory ataxia, other than neuropathic pain are the typical symptoms appearing in high rates of patients receiving cumulative doses of CDDP.^{3,10}

The key result of this work is the demonstration of a relation between the development of a severe painful-CIPN and extensive

angiogenesis of peripheral and central districts of nociception such as the lumbar dorsal root ganglia (L4-L6 DRG), the lumbar spinal cord (at L4-L5) and the primary somatosensory cortex (S1). Specifically, we found that PTX-induced painful neuropathy is significantly linked with angiogenesis in the DRG, L4-L5 DRG and S1 cortex while CDDP-induced non-painful neuropathy was not. In addition, a consistent reduction of the average vascular diameter, in all three regions of PTX-treated animals, testified that angiogenesis was compatible with the formation of smaller capillaries, in comparison to vehicle groups, by sprouting processes. Other measurements on the reconstructed

vascular systems revealed that in the PTX group novel vessels were also less distributed over the tissue because tortuosity decreased throughout.

A certain extent of tortuosity is necessary for capillaries to best serve the contingent local blood volume; therefore, a tortuosity reduction indicates a loss of efficiency in nutrient delivery by capillaries. Moreover, vessels of the PTX group had many more branches in DRG, L4-L5 and S1 supporting the hypothesis that sprouting angiogenesis has taken place.

Concerning the method of analysis of the vasculature, the XCPT analysis, it requires the Indian-ink perfusion of animals, well established and employed by other authors for decades. Details on the analysis previously evidenced that (i) no leakage is due to the dye; (ii) Indian-ink preparation is not compatible with immunostaining, though; (iii) vessels with lumen larger than 100 microns (arterioles and venules) are hardly stained because of the low viscosity of the dye.⁴⁴⁻⁴⁷

Similar results were obtained also after nerve ligation, where we observed an early diffuse and conspicuous microvascular neogenesis mainly in the primary somatosensory cortex compared to other brain regions of neuropathic animals, already peaking at 15 days from the nerve lesion. Progressive fading of this microvessel neogenesis then ensued in the next 6 months, yet maintaining higher vascular density with a preserved small fraction of them.⁴⁸

In the present work, the significant differences in neovasculature emerged almost only in the PTX group, but also CDDP animals showed a similar trend when comparing morphological metrics like tortuosity and branching. This could mean that some modifications occur as well in non-painful milder CIPN, but they were not strong enough to produce important vascular remodelling. Therefore, angiogenesis into the somatosensory pathway could be a specific footprint of painful neuropathies.

From our analyses, specific regions seem to be differentially affected by angiogenesis. Indeed, the primary somatosensory cortex resulted in the largest effect sizes within regional comparisons followed by the lumbar spinal tract and by the DRG. This appeared counterintuitive because in the somatosensory and the nociceptive ascendant pathway, DRG is firstly involved in gathering, processing and routing of the hyperactivity induced by peripheral neuropathy, subsequently followed by the spinal cord and eventually the somatotopic cortical area. However, it should be noticed that as neurons and glial cells are much more prone to changes (i.e., plasticity) in the cerebral cortex, vascular endothelium could be more favourable to adaptive modifications in the central regions than in the peripheral districts. A previous study on the vascular architecture of DRG demonstrated a high neovascularisation after nerve injury, with a high degree of vascular branching, irregularity, and tortuosity in DRG ipsilateral to the damage.³³

In our hypothesis, angiogenesis could be a subtle consequence of the neuronal hyperactivity and hyperexcitability induced by peripheral neuropathy. More in detail, the prolonged increased activity of the ascending somatosensory pathway⁴⁹ generates a condition of nutrients and metabolites deficiency that is typically accompanied by

upregulation of hypoxic factors (e.g., the hypoxic inducible factor 1a)^{49,50} that, in turn, is generally associated with the upregulation of pro-angiogenic genes like the vascular endothelial growth factor (e.g., the VEGF family) and the angiotensin.^{51,52} VEGF would probably play a key role: for example, it was demonstrated that VEGF and its receptor flk-1 are overexpressed in the DRG following peripheral mechanical nerve injury^{53,54} and in spinal cord after compression.⁵⁵ Moreover VEGF is a potent angiogenic factor that stimulates the formation of new blood vessels *in vivo* and enhances vascular permeability (for details, see the study by Lange et al.⁵⁶). Moreover, VEGF is a neurotrophic factor that can stimulate axonal outgrowth, neuron survival and Schwann cell proliferation.^{53,54}

According to this thread, angiogenesis would be a fast and adaptive response to best preserve neuron structure and function by increasing the energy supply to the aberrant neuronal populations. A relation between the neuroprotective role of angiogenesis and peripheral neuropathy is not new. In fact, authors found that systemic administration of antagonists of VEGFR1 aggravated PTX-induced neuropathy in the DRG of mice.⁵⁷ Oppositely, injection of VEGF-A (one of the prominent pro-angiogenic factors) in the knee seems sufficient to cause osteoarthritis in wild-type mice.⁵⁸ A similar result emerged from VEGF-A injections into the temporomandibular joint.⁵⁹ Therefore, the role of angiogenesis, and its promoting factors, appears controversial in diverse neuropathic pain conditions.⁶⁰ A potential explanation of such an antithetical role could be the temporal development of the pro-angiogenic profile during the evolution of neuropathy. Indeed, while at early stages angiogenesis could serve as neuroprotection, lately it could contribute to the maintenance of the chronic conditions induced by neuropathy.

One obvious limitation of this work is represented by the lack of information regarding the functionality of the neogenerated vessels in the central and peripheral districts of PTX-treated animals. In other terms, at this point, we cannot affirm whether the vessels are functional in optimally perfusing the tissue with metabolites and oxygen, thus whether novel vessels take part in the blood flow dynamics. Moreover, the newly formed vessels appeared to be less tortuous, suggesting a weak and less effective spread of nutrients and metabolites in the tissue. An altered vascularisation in the PNS can have an indirect role in the processes of degeneration of nerve tissue, triggered by direct exposure to chemotherapy, almost indirectly.

Literature data reported that several pathological pathways seem to be activated in neurons and supportive glial cells in the PNS and CNS after treatment with neurotoxic chemotherapy; this is related to an impaired microtubule assembly and disassembly, impaired axonal transport and vesicle trafficking, impaired intracellular calcium, mitochondrial alterations, ATP deficits, bioenergetic failure and the generation of Oxygen Radical Species (for a review, see the study by Velasco-González and Coffeen⁶¹). Moreover, the secretion of hyperactivating neuropeptides (substance P and calcitonin gene-related peptide) from peripheral and central neurons⁶²⁻⁶⁴ determine, as a cascade process, an increasing neuronal hypersensitisation that triggers the onset and development of painful conditions. The involvement of

altered vascularisation, blood supply and oxygen/nutrients/metabolites in this scenario remains to be elucidated.

Moreover, also the integrity of the barrier generated by endothelial cells (i.e., blood–brain barrier) in these newly formed vessels in the CNS has to be verified. The massive and dis-homogeneous creation of new vessels in specific regions of the brain and the spinal cord could lead to defective endothelial barriers.

The immediate consequence of our results is the possibility of regulating micro-angiogenesis in order to control the pain development in chemotherapy-induced neuropathy. The literature data reflect the controversial implications of VEGF in nociception since both pro- and anti-nociceptive activities have been described. As examples, to support the hypothesis that decreasing the levels of VEGF may cause hyperalgesia, Verheyen et al.⁵⁷ demonstrated that the neutralisation of all endogenous VEGF isoforms, or VEGF receptor antagonism increases pain sensitivity in PTX-induced neuropathy. To support the contrary hypothesis, Ludin et al. demonstrated that the anti-VEGF receptor treatment can alleviate the neuropathic pain in chronic constriction injury rats, by decreasing the expression of VEGF and purinergic P2X2/3 receptors in DRG neurons.⁵⁸ Besides the nociception, Kirchmair et al.^{65,66} demonstrated a degeneration of the vasa nervorum after treatment with PTX and CDDP that can be prevented by the co-administration of the DNA encoding VEGF-1, suggesting a positive role of VEGF on the recovery of vascularity and, consequently, an improved nerve functionality in toxic neuropathies. Moreover, Micheli et al.²⁵ proved that an increase in VEGF-A can be involved in oxaliplatin-induced neuropathic pain and could be mitigated by VEGF-A antibodies in an animal model of painful toxic neuropathy. The potential of VEGF-A to be alternatively spliced into two families of splice variants with opposite effects⁶⁷ can justify these controversial results. A pro-nociceptive and an anti-nociceptive variant have been detected in rats with saphenous nerve injury (where the pro-nociceptive variant was prevalent) and in diabetic neuropathic rats (where the anti-nociceptive variant) was prevalent.^{68,69}

The demonstration of the increased angiogenesis in the CNS and PNS of rats with severe painful peripheral neuropathy (PTX model) and not in rats with painless neurotoxicity (CDDP model), reported in the present work, inspires the possibility that an anti-angiogenic treatment can avoid the painful consequences of the treatment with toxic antineoplastic agents, opening new possibilities for the treatment of neurotoxicity and neuropathic pain. However, it will be of crucial importance to determine the timing of the onset of vascular alterations during the development of neuropathic symptoms, in order to determine the optimal time of exposure and dosage of the anti-angiogenic treatment. Moreover, importantly, the neo-angiogenic pathways need to be elucidated also. In this scenario, the documented antineoplastic effect of anti-angiogenic compounds excludes any impacting effects on the antitumoral activity of chemotherapy drugs. The administration of PTX, in combination with bevacizumab, has been extensively reported as a safe therapeutic schedule against several solid tumours (for reviews see the studies by Croom and Dhillon⁷⁰ and Rosen et al.⁷¹).

5 | CONCLUSION

In conclusion, in this work, we described, by synchrotron radiation-X-ray computer-assisted microtomography, abundant angiogenesis in the CNS and PNS of rats with severe painful-CIPN, with alterations in the complexity of the vascular network. These results can shed light on new factors involved in the development of neurotoxicity and neuropathic pain after peripheral nerve damage.

FUNDING INFORMATION

This study was supported by Italian Ministry of University and Research (PRIN Progetti di Ricerca di Interesse Nazionale, 2022, Recipient Valentina Alda Carozzi, Prot No. 2022NBS28K); FAR 2022–2021 University Grants (recipient Valentina Alda Carozzi); AIRC grant no. IG2021, ID# 2578 (recipient Guido Cavaletti); National Plan for NRRP Complementary Investments (PNC, established with the decree-law 6 May 2021, no. 59, converted by law no. 101 of 2021) in the call for the funding of research initiatives for technologies and innovative trajectories in the health and care sectors (Directorial Decree no. 931 of 06-06-2022)—project no. PNC0000003—AdvaNced Technologies for Human-centrEd Medicine (project acronym: ANTHEM, recipient Guido Cavaletti). This work reflects only the authors' views and opinions, neither the Ministry for University and Research nor the European Commission can be considered responsible for them.

DATA AVAILABILITY STATEMENT

The data that support the findings of this study are available on request from the corresponding author. The data are not publicly available due to privacy or ethical restrictions.

ORCID

Paola Alberti  <https://orcid.org/0000-0001-6106-6183>

Cristina Meregalli  <https://orcid.org/0000-0002-4281-4577>

Guido Cavaletti  <https://orcid.org/0000-0003-4128-2406>

Valentina Alda Carozzi  <https://orcid.org/0000-0003-0963-7107>

REFERENCES

1. Alberti P, Cavaletti G, Cornblath DR. Toxic neuropathies: chemotherapy induced peripheral neurotoxicity. *Curr Opin Neurol*. 2019;32(55):676–683. doi:10.1097/WCO.0000000000000724
2. Sařat K. Chemotherapy-induced peripheral neuropathy: part 1-current state of knowledge and perspectives for pharmacotherapy. *Pharmacol Rep*. 2020;72(3):486–507. doi:10.1007/s43440-020-00109-y
3. Alberti P, Salvalaggio A, Argyriou AA, et al. Neurological complications of conventional and novel anticancer treatments. *Cancer*. 2022;14(24):1–25. doi:10.3390/cancers14246088
4. Loprinzi CL, Lacchetti C, Bleeker J, et al. Prevention and management of chemotherapy-induced peripheral neuropathy in survivors of adult cancers: ASCO guideline update. *J Clin Oncol*. 2020;38(28):3325–3348. doi:10.1200/JCO.20.01399
5. Staff NP, Grisold A, Grisold W, Windebank AJ. Chemotherapy-induced peripheral neuropathy: a current review. *Ann Neurol*. 2017;81(6):772–781. doi:10.1002/ana.24951

6. Attal N, Cruccu G, Baron R, et al. EFNS guidelines on the pharmacological treatment of neuropathic pain: 2010 revision. *Eur J Neurol*. 2010;17(9):1113-1123. doi:[10.1111/j.1468-1331.2010.02999.x](https://doi.org/10.1111/j.1468-1331.2010.02999.x)
7. Bates D, Carsten Schultheis B, Hanes MC, et al. A comprehensive algorithm for management of neuropathic pain. *Pain Med*. 2019;20:S2-S12. doi:[10.1093/pm/pnz075](https://doi.org/10.1093/pm/pnz075)
8. Dworkin RH, O'Connor AB, Kent J, et al. Interventional management of neuropathic pain: NeuPSIG recommendations. *Pain*. 2013;154(11):2249-2261. doi:[10.1016/j.pain.2013.06.004](https://doi.org/10.1016/j.pain.2013.06.004)
9. Stucky CL, Mikesell AR. Cutaneous pain in disorders affecting peripheral nerves. *Neurosci Lett*. 2021;765:136233. doi:[10.1016/j.neulet.2021.136233](https://doi.org/10.1016/j.neulet.2021.136233)
10. Park SB, Krishnan AV, Lin CS, Goldstein D, Friedlander M, Kiernan MC. Mechanisms underlying chemotherapy-induced neurotoxicity and the potential for neuroprotective strategies. *Curr Med Chem*. 2008;15(29):3081-3094. doi:[10.2174/092986708786848569](https://doi.org/10.2174/092986708786848569)
11. Klein I, Lehmann HC. Pathomechanisms of paclitaxel-induced peripheral neuropathy. *Toxics*. 2021;9(10):229. doi:[10.3390/toxics9100229](https://doi.org/10.3390/toxics9100229)
12. Bae EH, Greenwald MK, Schwartz AG. Chemotherapy-induced peripheral neuropathy: mechanisms and therapeutic avenues. *Neurotherapeutics*. 2021;18(4):2384-2396. doi:[10.1007/s13311-021-01142-2](https://doi.org/10.1007/s13311-021-01142-2)
13. Zajączkowska R, Kocot-Kępska M, Leppert W, Wrzosek A, Mika J, Wordliczek P. Mechanisms of chemotherapy-induced peripheral neuropathy. *J Int J Mol Sci*. 2019;20(6):1451. doi:[10.3390/ijms20061451](https://doi.org/10.3390/ijms20061451)
14. Argyriou AA, Bruna J, Park SB, Cavaletti G. Emerging pharmacological strategies for the management of chemotherapy-induced peripheral neurotoxicity (CIPN), based on novel CIPN mechanisms. *Expert Rev Neurother*. 2020;20:1005-1016. doi:[10.1080/14737175.2020.1796639](https://doi.org/10.1080/14737175.2020.1796639)
15. Carozzi VA, Canta A, Chiorazzi A. Chemotherapy-induced peripheral neuropathy: what do we know about mechanisms? *Neurosci Lett*. 2015;596:90-107. doi:[10.1016/j.neulet.2014.10.014](https://doi.org/10.1016/j.neulet.2014.10.014)
16. Carozzi V, Chiorazzi A, Canta A, et al. Effect of the chronic combined administration of cisplatin and paclitaxel in a rat model of peripheral neurotoxicity. *Eur J Cancer*. 2009;45(4):656-665. doi:[10.1016/j.ejca.2008.10.038](https://doi.org/10.1016/j.ejca.2008.10.038)
17. Cavaletti G, Marmiroli P, Renn CL, et al. Cannabinoids: an effective treatment for chemotherapy-induced peripheral neurotoxicity? *Neurotherapeutics*. 2021;18(4):2324-2336. doi:[10.1007/s13311-021-01127-1](https://doi.org/10.1007/s13311-021-01127-1)
18. Chua KC, El-Haj N, Priotti J, Kroetz DL. Mechanistic insights into the pathogenesis of microtubule-targeting agent-induced peripheral neuropathy from pharmacogenetic and functional studies. *Basic Clin Pharmacol Toxicol*. 2022;130(S1):60-74. doi:[10.1111/bcpt.13654](https://doi.org/10.1111/bcpt.13654)
19. Doyle TM, Salvemini D. Mini-review: mitochondrial dysfunction and chemotherapy-induced neuropathic pain. *Neurosci Lett*. 2021;760:136087. doi:[10.1016/j.neulet.2021.136087](https://doi.org/10.1016/j.neulet.2021.136087)
20. Fumagalli G, Monza L, Cavaletti G, Rigolio R, Meregalli C. Neuroinflammatory process involved in different preclinical models of chemotherapy-induced peripheral neuropathy. *Front Immunol*. 2021;11:1-29. doi:[10.3389/fimmu.2020.626687](https://doi.org/10.3389/fimmu.2020.626687)
21. Meregalli C, Bonomo R, Cavaletti G, Carozzi VA. Blood molecular biomarkers for chemotherapy-induced peripheral neuropathy: from preclinical models to clinical practice. *Neurosci Lett*. 2021;749:135739. doi:[10.1016/j.neulet.2021.135739](https://doi.org/10.1016/j.neulet.2021.135739)
22. Meregalli C, Fumagalli G, Alberti P, et al. Neurofilament light chain: a specific serum biomarker of axonal damage severity in rat models of chemotherapy-induced peripheral neurotoxicity. *Arch Toxicol*. 2020;94(7):2517-2522. doi:[10.1007/s00204-020-02755-w](https://doi.org/10.1007/s00204-020-02755-w)
23. Di Cesare Mannelli L, Pacini A, Bonaccini L, Zanardelli M, Mello T, Ghelardini C. Morphologic features and glial activation in rat oxaliplatin-dependent neuropathic pain. *J Pain*. 2013;14(12):1585-1600. doi:[10.1016/j.jpain.2013.08.002](https://doi.org/10.1016/j.jpain.2013.08.002)
24. Lee JH, Kim W. The role of satellite glial cells, astrocytes, and microglia in oxaliplatin-induced neuropathic pain. *Biomedicine*. 2020;8(9):1-23. doi:[10.3390/biomed8090324](https://doi.org/10.3390/biomed8090324)
25. Micheli L, Parisio C, Lucarini E, et al. VEGF-A/VEGFR-1 signalling and chemotherapy-induced neuropathic pain: therapeutic potential of a novel anti-VEGFR-1 monoclonal antibody. *J Exp Clin Cancer Res*. 2021;40(1):320. doi:[10.1186/s13046-021-02127-x](https://doi.org/10.1186/s13046-021-02127-x)
26. Pozzi E, Ballarini E, Rodriguez-Menendez V, et al. Paclitaxel, but not cisplatin, affects satellite glial cells in dorsal root ganglia of rats with chemotherapy-induced peripheral neurotoxicity. *Toxics*. 2023;11(2). doi:[10.3390/toxics11020093](https://doi.org/10.3390/toxics11020093)
27. Schmitt LI, Leo M, Kutritz A, Kleinschnitz C, Hagenacker T. Activation and functional modulation of satellite glial cells by oxaliplatin lead to hyperexcitability of sensory neurons in vitro. *Mol Cell Neurosci*. 2020;105:103499. doi:[10.1016/j.mcn.2020.103499](https://doi.org/10.1016/j.mcn.2020.103499)
28. Lees JG, Makker PG, Tonkin RS, et al. Immune-mediated processes implicated in chemotherapy-induced peripheral neuropathy. *Eur J Cancer*. 2017;73:22-29. doi:[10.1016/j.ejca.2016.12.006](https://doi.org/10.1016/j.ejca.2016.12.006)
29. Makker PG, Duffy SS, Lees JG, et al. Characterisation of immune and neuroinflammatory changes associated with chemotherapy-induced peripheral neuropathy. *PLoS One*. 2017;12(1):e0170814. doi:[10.1371/journal.pone.0170814](https://doi.org/10.1371/journal.pone.0170814)
30. Ollodart J, Steele LR, Romero-Sandoval EA, Strowd RE, Shiozawa Y. Contributions of neuroimmune interactions to chemotherapy-induced peripheral neuropathy development and its prevention/therapy. *Biochem Pharmacol*. 2024;222:116070. doi:[10.1016/j.bcp.2024.116070](https://doi.org/10.1016/j.bcp.2024.116070)
31. Carmeliet P. Angiogenesis in health and disease. *Nat Med*. 2003;9(6):653-660. doi:[10.1038/nm0603-653](https://doi.org/10.1038/nm0603-653)
32. Greenberg DA, Jin K. From angiogenesis to neuropathology. *Nature*. 2005;438(7070):954-959. doi:[10.1038/nature04481](https://doi.org/10.1038/nature04481)
33. Kubiček L, Kopáček R, Klusáková I, Dubový P. Alterations in the vascular architecture of the dorsal root ganglia in a rat neuropathic pain model. *Ann Anat*. 2010;192(2):101-106. doi:[10.1016/j.aanat.2010.01.005](https://doi.org/10.1016/j.aanat.2010.01.005)
34. Patera A, Zippo AG, Bonnin A, Stampanoni M, Biella GEM. Brain micro-vasculature imaging: an unsupervised deep learning algorithm for segmenting mouse brain volume probed by high-resolution phase-contrast X-ray tomography. *Int J Imaging Syst Technol*. 2020;1211-1220. doi:[10.1002/ima.22520](https://doi.org/10.1002/ima.22520)
35. Monza L, Fumagalli G, Chiorazzi A, Alberti P. Translating morphology from bench side to bed side via neurophysiology: 8-min protocol for peripheral neuropathy research. *J Neurosci Methods*. 2021;363. doi:[10.1016/j.jneumeth.2021.109323](https://doi.org/10.1016/j.jneumeth.2021.109323)
36. Meregalli C, Canta A, Carozzi VA, et al. Bortezomib-induced painful neuropathy in rats: a behavioral, neurophysiological and pathological study in rats. *Eur J Pain*. 2010;14(4):343-350. doi:[10.1016/j.ejpain.2009.07.001](https://doi.org/10.1016/j.ejpain.2009.07.001)
37. Meijer C, De Vries EG, Marmiroli P, Tredici G, Frattola L, Cavaletti G. Cisplatin-induced DNA-platination in experimental dorsal root ganglia neuronopathy. *Neurotoxicology*. 1999;20(6):883-887.
38. Chiorazzi A, Wozniak KM, Rais R, et al. Ghrelin agonist HM01 attenuates chemotherapy-induced neurotoxicity in rodent models. *Eur J Pharmacol*. 2018;840:89-103.
39. Dullin C, di Lillo F, Svetlove A, et al. Multiscale biomedical imaging at the SYRMEP beamline of Elettra—closing the gap between preclinical research and patient applications. *Physics Open*. 2021;6:100050. doi:[10.1016/j.physo.2020.100050](https://doi.org/10.1016/j.physo.2020.100050)
40. Brun F, Massimi L, Fratini M, et al. SYRMEP Tomo project: a graphical user interface for customizing CT reconstruction workflows. *Adv Struct Chem Imaging*. 2017;3(1):4. doi:[10.1186/s40679-016-0036-8](https://doi.org/10.1186/s40679-016-0036-8)
41. Bonomo R, Canta A, Chiorazzi A, et al. Effect of age on metabolomic changes in a model of paclitaxel-induced peripheral neurotoxicity. *J Peripher Nerv Syst*. 2023;29:58-71. doi:[10.1111/jns.12609](https://doi.org/10.1111/jns.12609)
42. Cata JP, Weng HR, Dougherty PM. Behavioral and electrophysiological studies in rats with cisplatin-induced chemoneuropathy. *Brain Res*. 2008;16(1230):91-98. doi:[10.1016/j.brainres.2008.07.022](https://doi.org/10.1016/j.brainres.2008.07.022)

43. Joseph EK, Levine JD. Comparison of oxaliplatin- and cisplatin-induced painful peripheral neuropathy in the rat. *J Pain*. 2009;10(5):534-541. doi:10.1016/j.jpain.2008.12.003
44. Duvernoy HM, Delon S, Vannson JL. Cortical blood vessels of the human brain. *Brain Res Bull*. 1981;7:519-579.
45. Reina-De La Torre F, Rodriguez-Baeza A, Sahuquillo-Barris J. Morphological characteristics and distribution pattern of the arterial vessels in human cerebral cortex: a scanning electron microscope study. *Anat Rec*. 1998;251:87-96.
46. Weber B, Keller AL, Reichold J, Logothetis NK. The microvascular system of the striate and extrastriate visual cortex of the macaque. *Cereb Cortex*. 2008;18:2318-2330.
47. Xue S, Gong H, Jiang T, et al. Indian-ink perfusion based method for reconstructing continuous vascular networks in whole mouse brain. *PLoS One*. 2014;9(1):e88067. doi:10.1371/journal.pone.0088067
48. Zippo AG, Del Grosso V, Patera A, et al. Chronic pain alters microvascular architectural organization of somatosensory cortex. 2019. doi:10.1101/755132
49. Kanngiesser M, Mair N, Lim HY, et al. Hypoxia-inducible factor 1 regulates heat and cold pain sensitivity and persistence. *Antioxid Redox Signal*. 2014;20(16):2555-2571. doi:10.1089/ars.2013.5494
50. Rojas DR, Tegeder I, Kuner R, Agarwal N. Hypoxia-inducible factor 1 α protects peripheral sensory neurons from diabetic peripheral neuropathy by suppressing accumulation of reactive oxygen species. *J Mol Med*. 2018;96(12):1395-1405. doi:10.1007/s00109-018-1707-9
51. Ciarlillo D, Celeste C, Carmeliet P, Boerboom D, Theoret C. A hypoxia response element in the Vegfa promoter is required for basal Vegfa expression in skin and for optimal granulation tissue formation during wound healing in mice. *PLoS One*. 2017;12(7):e0180586. doi:10.1371/journal.pone.0180586
52. Ramakrishnan S, Anand V, Roy S. Vascular endothelial growth factor signaling in hypoxia and inflammation. *J Neuroimmune Pharmacol*. 2014;9(2):142-160. doi:10.1007/s11481-014-9531-7
53. Sondell M, Lundborg G, Kanje M. Vascular endothelial growth factor has neurotrophic activity and stimulates axonal outgrowth, enhancing cell survival and Schwann cell proliferation in the peripheral nervous system. *J Neurosci*. 1999;19(14):5731-5740. doi:10.1523/JNEUROSCI.19-14-05731.1999
54. Sondell M, Sundler F, Kanje M. Vascular endothelial growth factor is a neurotrophic factor which stimulates axonal outgrowth through the flk-1 receptor. *Eur J Neurosci*. 2000;12(12):4243-4254. doi:10.1046/j.0953-816x.2000.01326.x
55. Watanabe T. Is vascular endothelial cell growth factor (VEGF) involved in the pathogenesis of diabetic nephropathy? *Nephrology (Carlton)*. 2007;12(Suppl 3):S27. doi:10.1111/j.1440-1797.2007.00879_2.x
56. Lange C, Storkebaum E, de Almodóvar CR, Dewerchin M, Carmeliet P. Vascular endothelial growth factor: a neurovascular target in neurological diseases. *Nat Rev Neurol*. 2016;12(8):439-454. doi:10.1038/nrneurol.2016.88
57. Verheyen A, Peeraer E, Nuydens R, et al. Systemic anti-vascular endothelial growth factor therapies induce a painful sensory neuropathy. *Brain*. 2012;135(9):2629-2641. doi:10.1093/brain/aws145
58. Ludin A, Sela JJ, Schroeder A, Samuni Y, Nitzan DW, Amir G. Injection of vascular endothelial growth factor into knee joints induces osteoarthritis in mice. *Osteoarthr Cartil*. 2013;21(3):491-497. doi:10.1016/j.joca.2012.12.003
59. Shen P, Jiao Z, Zheng JS, et al. Injecting vascular endothelial growth factor into the temporomandibular joint induces osteoarthritis in mice. *Sci Rep*. 2015;5. doi:10.1038/srep16244
60. Hamilton JL, Nagao M, Levine BR, Chen D, Olsen BR, Im H-J. Targeting VEGF and its receptors for the treatment of osteoarthritis and associated pain. *J Bone Miner Res*. 2016;31(5):911-924. doi:10.1002/jbmr.2828
61. Velasco-González R, Coffeen U. Neurophysiopathological aspects of paclitaxel-induced peripheral neuropathy. *Neurotox Res*. 2022;40(6):1673-1689. doi:10.1007/s12640-022-00582-8
62. Chiba T, Oka Y, Kambe T, et al. Paclitaxel-induced peripheral neuropathy increases substance P release in rat spinal cord. *Eur J Pharmacol*. 2016;770:46-51. doi:10.1016/j.ejphar.2015.11.055
63. Pittman SK, Gracias NG, Vasko MR, Fehrenbacher JC. Paclitaxel alters the evoked release of calcitonin gene-related peptide from rat sensory neurons in culture. *Exp Neurol*. 2014;253:146-153. doi:10.1016/j.expneurol.2013.12.011
64. Tatsushima Y, Egashira N, Kawashiri T, et al. Involvement of substance P in peripheral neuropathy induced by paclitaxel but not oxaliplatin. *J Pharmacol Exp Ther*. 2011;337(1):226-235. doi:10.1124/jpet.110.175976
65. Kirchmair R, Walter DH, Li M, et al. Antiangiogenesis mediates cisplatin-induced peripheral neuropathy: attenuation or reversal by local vascular endothelial growth factor gene therapy without augmenting tumor growth. *Circulation*. 2005;111(20):2662-2670. doi:10.1161/CIRCULATIONAHA.104.470849
66. Kirchmair R, Tietz AB, Panagiotou E, et al. Therapeutic angiogenesis inhibits or rescues chemotherapy-induced peripheral neuropathy: taxol- and thalidomide-induced injury of vasa nervorum is ameliorated by VEGF. *Mol Ther*. 2007;15(1):69-75. doi:10.1038/sj.mt.6300019
67. Woolard J, Wang WY, Bevan HS, et al. VEGF165b, an inhibitory vascular endothelial growth factor splice variant: mechanism of action, in vivo effect on angiogenesis and endogenous protein expression. *Cancer Res*. 2004;64(21):7822-7835. doi:10.1158/0008-5472.CAN-04-0934
68. Hulse RP, Beazley-Long N, Hua J, et al. Regulation of alternative VEGF-A mRNA splicing is a therapeutic target for analgesia. *Neurobiol Dis*. 2014;71:245-259. doi:10.1016/j.nbd.2014.08.012
69. Hulse RP, Beazley-Long N, Ved N, et al. Vascular endothelial growth factor-A165b prevents diabetic neuropathic pain and sensory neuronal degeneration. *Clin Sci*. 2015;129(8):741-756. doi:10.1042/CS20150124
70. Croom KF, Dhillon S. Bevacizumab: a review of its use in combination with paclitaxel or capecitabine as first-line therapy for HER2-negative metastatic breast cancer. *Drugs*. 2011;71(16):2213-2229. doi:10.2165/11207720-000000000-00000
71. Rosen VM, Guerra I, McCormack M, et al. Systematic review and network meta-analysis of bevacizumab plus first-line topotecan-paclitaxel or cisplatin-paclitaxel versus non-bevacizumab-containing therapies in persistent, recurrent, or metastatic cervical cancer. *Int J Gynecol Cancer*. 2017;27(6):1237-1246. doi:10.1097/IGC.0000000000001000

SUPPORTING INFORMATION

Additional supporting information can be found online in the Supporting Information section at the end of this article.

How to cite this article: Zippo AG, Rodriguez-Menendez V, Pozzi E, et al. Paclitaxel alters the microvascular network in the central and peripheral nervous system of rats with chemotherapy-induced painful peripheral neuropathy. *J Peripher Nerv Syst*. 2024;29(4):537-554. doi:10.1111/jns.12660